

Temporally-Consistent Bilinearly Recurrent Autoencoders for Control Systems

Ananda Chakrabarti^{1*}, Indranil Nayak^{2*}, Debdipta Goswami³

Abstract—This paper introduces the temporally-consistent bilinearly recurrent autoencoder (tcBLRAN), a Koopman operator based neural network architecture for modeling a control-affine nonlinear control system. The proposed method extends traditional Koopman autoencoders (KAE) by incorporating bilinear recurrent dynamics that are consistent across predictions, enabling accurate long-term forecasting for control-affine systems. This overcomes the roadblock that KAEs face when encountered with limited and noisy training datasets, resulting in a lack of generalizability due to inconsistency in training data. Through a blend of deep learning and dynamical systems theory, tcBLRAN demonstrates superior performance in capturing complex behaviors and control systems dynamics, providing a superior data-driven modeling technique for control systems and outperforming the state-of-the-art Koopman bilinear form (KBF) learned by autoencoder networks.

I. INTRODUCTION

Accurate modeling and prediction of nonlinear dynamical systems with inputs represents a cornerstone challenge in control engineering. Traditional physics-based modeling is becoming increasingly challenging for complex nonlinear systems with insufficient system-level knowledge. On the other hand, recent developments in machine-learning (ML) techniques for modeling complex systems from data have become useful in a wide variety of problems, e.g., classification, speech recognition [1], board games [2], and even discovering mathematical algorithms [3]. However, any knowledge of the underlying dynamical system provides valuable insights to generate appropriate features and interpretability to any ML algorithm, giving rise to a family of physics constrained learning (PCL) methods that incorporate constraints arising from physical consistency of the governing dynamical system. In this context, the Koopman operator theory [4], [5] emerges as a powerful tool, offering a linear perspective on inherently nonlinear dynamical systems. This theory enables the application of linear analysis techniques to nonlinear systems by operating in an infinite-dimensional function space, thereby linearizing the dynamics of observable functions. However, since the Koopman operator generally maps between infinite-dimensional function spaces, it cannot

be represented computationally without a finite-dimensional projection. Early methods e.g., extended dynamic mode decomposition (EDMD) [6] use large amount of data to approximate the Koopman operator and the latent linear dynamics by projecting it on carefully crafted dictionary functions. But the goodness of the approximation depends on the Koopman-invariance property of the dictionary. More recently, a class of ML algorithms has been developed to automate the choice of dictionary by using deep neural networks (DNNs) to find an approximate finite-dimensional Koopman invariant subspace. These Koopman autoencoder (KAE) or linearly recurrent autoencoder (LRAN) algorithms use an autoencoder network that maps the state-space into a latent space where the dynamics can be linearly approximated by the finite-dimensional Koopman operator encoded via a linear layer [7], [8].

Despite the promising foundation laid by Koopman operator theory, its direct application to control systems poses significant challenges since the linear latent structure is no more valid with a time-varying control input. For a control-affine system, [9], [10] proves the latent dynamics to be bilinear in the Koopman invariant subspace, thereby yielding Koopman bilinear form (KBF). The KAE/LRAN framework is applied to learn KBF for robotic system control [11], but the window for accurate prediction remains short with control-input. In a recent work by the authors, temporally-consistent Koopman autoencoder (tcKAE) [12] is developed for consistent and accurate prediction of *autonomous* dynamical systems using a temporal consistency constraint with Koopman autoencoder framework. It compares the predictions from different initial time-instances to a final time in the latent space in contrast with prior KAE methodologies, where the enforcement of multi-step look-ahead prediction loss is reliant on *labelled* data and latent space representation of the labelled data.

This paper presents the temporally-consistent bilinearly recurrent autoencoders (tcBLRAN) for *control* systems by employing the temporal consistency regularization developed in [12] to learn the KBF using a bilinearly recurrent autoencoder. The contributions of this manuscript are: (1) extension of traditional KAE/LRAN to control-affine nonlinear systems with bilinear recurrent autoencoders, thereby enforcing the Koopman invariance conditions developed in [9]; (2) introduction of a prediction consistency mechanism that ensures the temporal coherence of model predictions, significantly enhancing long-term forecasting accuracy; (3) provide a theoretical justification to the prediction consistency from the time-invariance property of the control system; (4) comprehensive evaluation of the model-prediction performance

This work is supported by OSU Departmental Startup fund.

¹Ananda Chakrabarti is a PhD student in the Department of Electrical and Computer Engineering, The Ohio State University, Columbus, OH 43210. chakrabarti.44@osu.edu

²Indranil Nayak is a PhD Candidate in the Department of Electrical and Computer Engineering, The Ohio State University, Columbus, OH 43210. nayak.77@osu.edu

³Debdipta Goswami is an Assistant Professor in the Department of Mechanical and Aerospace Engineering, The Ohio State University, Columbus, OH 43210. goswami.78@osu.edu

*First two authors contributed equally to this manuscript.

of tcBLRAN and vanilla BLRAN for different control-affine nonlinear systems.

By bridging the gap between KAE and control-affine systems, tcBLRAN not only broadens the applicability of Koopman-based models but also sets a new benchmark in the predictive modeling of dynamic systems. Our contributions pave the way for future advancements in control theory, predictive modeling, and beyond, promising significant implications for a wide array of applications ranging from autonomous vehicles to energy management systems.

The paper is organized as follows: Section II provides an overview of Koopman spectral theory, describes Koopman bilinear form, and introduces Koopman autoencoders for dynamics learning. Section III proposes the tcBLRAN algorithm and provides its theoretical basis. Section IV illustrates the prediction performance with numerical examples. Section V summarizes the paper and suggests possible future work.

II. MATHEMATICAL PRELIMINARIES

A. Koopman theory: an overview

Consider a dynamical system evolving on a compact manifold $\mathbb{X} \subseteq \mathbb{R}^d$,

$$\dot{\mathbf{x}} = \mathbf{f}(\mathbf{x}), \quad (1)$$

where $\mathbf{x} \in \mathbb{X}$ and $\mathbf{f} : \mathbb{X} \rightarrow \mathbb{X}$. Let $\Phi(t, \mathbf{x})$ be the flow map of the system (1) at time $t > 0$ starting from an initial state \mathbf{x} . A measurable function $\varphi : \mathbb{X} \rightarrow \mathbb{C}$ is called an observable of the dynamical system (1). Let \mathcal{F} be the space of all complex-valued observables $\varphi : \mathbb{X} \rightarrow \mathbb{C}$. The continuous-time Koopman operator is defined as $\mathcal{K}^t : \mathcal{F} \rightarrow \mathcal{F}$ such that

$$(\mathcal{K}^t \varphi)(\cdot) = \varphi \circ \Phi(t, \cdot), \quad (2)$$

where \circ denotes the function composition. Unlike the original system, the Koopman operator is linear over its arguments, i.e., observable functions, and therefore can be characterized by its eigenvalues and eigenfunctions. A function $\phi : \mathbb{X} \rightarrow \mathbb{C}$ is an eigenfunction of \mathcal{K}^t if

$$(\mathcal{K}^t \phi)(\cdot) = e^{\lambda t} \phi(\cdot), \quad (3)$$

with eigenvalue $\lambda \in \mathbb{C}$. The infinitesimal generator of \mathcal{K}^t , i.e., $\lim_{t \rightarrow 0} \frac{\mathcal{K}^t - I}{t}$, is $\mathbf{f} \cdot \nabla = L_{\mathbf{f}}$ [13], where I is the identity operator and $L_{\mathbf{f}}$ is the Lie derivative with respect to \mathbf{f} . The infinitesimal generator satisfies the eigenvalue equation

$$L_{\mathbf{f}} \phi = \lambda \phi. \quad (4)$$

Hence, the time-varying observable $\psi(t, \mathbf{x}) \triangleq \mathcal{K}^t \varphi(\mathbf{x})$ is the solution of the partial differential equation (PDE) [13]

$$\begin{aligned} \frac{\partial \psi}{\partial t} &= L_{\mathbf{f}} \psi, \\ \psi(0, \mathbf{x}) &= \varphi(\mathbf{x}). \end{aligned} \quad (5)$$

In spite of its linearity, the Koopman operator is infinite-dimensional and has an infinite number of eigenfunctions. In fact, if ϕ_1 and ϕ_2 are eigenfunctions of \mathcal{K}^t with eigenvalues λ_1 and λ_2 , respectively, then $\phi_1^k \phi_2^l$ is also an eigenfunction with eigenvalue $k\lambda_1 + l\lambda_2$ for any $k, l \in \mathbb{N}$. Moreover, the

Koopman operator, being infinite-dimensional, may contain continuous and residual spectra with a generalized eigendistribution [14]. However, the discussions in this paper are restricted to the point spectra of the Koopman operator.

Let $\mathbf{g}(\cdot) \in \mathcal{F}^p$, $p \in \mathbb{N}$, be a vector-valued observable. The observable \mathbf{g} can be expressed in terms of Koopman eigenfunctions $\phi_i(\cdot)$ as follows:

$$\mathbf{g}(\cdot) = \sum_{i=1}^{\infty} \phi_i(\cdot) \mathbf{v}_i^{\mathbf{g}}, \quad (6)$$

where $\mathbf{v}_i^{\mathbf{g}} \in \mathbb{R}^p$, $i = 1, 2, \dots$, are called the *Koopman modes* of the observable $\mathbf{g}(\cdot)$. Koopman modes form the projection of the observable on the span of Koopman eigenfunctions [15]. The Koopman eigenvalues and eigenfunctions are properties of the dynamics only, whereas the Koopman modes depend on the observable.

B. Koopman bilinear form: Koopman approximation of control affine system

Consider the control affine system

$$\begin{aligned} \dot{\mathbf{x}} &= \mathbf{f}(\mathbf{x}) + \sum_{i=1}^m \mathbf{g}_i(\mathbf{x}) u_i \\ \mathbf{y} &= \mathbf{h}(\mathbf{x}), \quad \mathbf{x}_{t_0} = \mathbf{x}_0, \end{aligned} \quad (7)$$

where $\mathbf{x} \in \mathbb{X} \subseteq \mathbb{R}^d$, $u_i \in \mathbb{R}$, for $i = 1, \dots, m$ and $\mathbf{y} \in \mathbb{R}^p$. Here the control input enters only through the control vector fields \mathbf{g}_i . Applying (5) to the system (7), the evolution of the PDE, derived in [16], is

$$\begin{aligned} \frac{\partial \psi}{\partial t} &= L_{\mathbf{f}} \psi + \sum_{i=1}^m u_i L_{\mathbf{g}_i} \psi, \\ \psi(0, \mathbf{x}) &= \varphi(\mathbf{x}), \end{aligned} \quad (8)$$

where $L_{\mathbf{g}_i} \triangleq \mathbf{g}_i \cdot \nabla$, $i = 1, \dots, m$ are the corresponding Lie derivatives and hence are linear operators on the space of ψ . The resultant bilinear forced PDE system (8) provides a way to represent the control-affine system (7) in a lifted latent space as a bilinear ODE. The following theorem from [16], [9] provides the sufficient condition for bilinearization of (7):

Theorem 1. [16], [9] The system (7) is bilinearizable in a countable (possibly infinite) basis if the eigenspace of $L_{\mathbf{f}}$, i.e., the Koopman generator corresponding to the drift vector field is an invariant subspace of $L_{\mathbf{g}_i}$, $i = 1, \dots, m$, i.e., the Koopman generators related to the control vector fields.

Remark 1. This result is further extended in [10] for any invariant subspace of $L_{\mathbf{f}}$, i.e., any Koopman-invariant subspace associated with the drift vector field that is invariant under $L_{\mathbf{g}_i}$, $i = 1, \dots, m$, thereby removing the necessity to find Koopman eigenfunctions.

References [9], [10] further demonstrates that if a transformation $\Psi(\cdot) \in \mathcal{F}^{N_i}$, $\Psi(\cdot) = [\psi_1(\cdot), \dots, \psi_{N_i}(\cdot)]^T$ can be found such that $\text{span}\{\psi_1(\cdot), \dots, \psi_{N_i}(\cdot)\}$ is invariant under $L_{\mathbf{f}}$ and $L_{\mathbf{g}_i}$, $i = 1, \dots, m$, then the transformation $\mathbf{z} = \Psi(\mathbf{x})$ allows us to express the system (7) in the following Koopman

bilinear form (KBF)

$$\dot{\mathbf{z}} = A\mathbf{z} + \sum_{i=1}^m B_i \mathbf{z} u_i, \quad (9)$$

where A and B_i 's are the approximation of Koopman generators for drift and control-vector fields.

C. Enforcing invariance via neural-networks: Koopman autoencoders

Discovering a finite-dimensional Koopman-invariant subspace purely from data is a challenging task, and an active area of research. Recent works [17], [8], [7] leverage the non-linear function approximation capabilities of neural networks to find a suitable transformation from the state space \mathbb{X} to a Koopman invariant subspace via latent state \mathbf{z} . The basic operation of KAE can be decomposed into three components (10), *i*) an encoding ($\Psi_e(\cdot) : \mathbb{X} \rightarrow \mathbb{R}^{N_l}$) that transforms the original state \mathbf{x} to a Koopman observable $\mathbf{z} \in \mathbb{R}^{N_l}$, *ii*) advancing the dynamics in that transformed space through a linear operator ($K^{\Delta t} \in \mathbb{R}^{N_l \times N_l}$), and *iii*) a decoding ($\Psi_d(\cdot)$) back to the original state space:

$$\begin{aligned} \mathbf{z}_t \approx \Psi_e(\mathbf{x}_t) &\rightarrow \mathbf{z}_{t+\Delta t} = K^{\Delta t} \cdot \mathbf{z}_t \\ &\rightarrow \mathbf{x}_{t+\Delta t} \approx \Psi_d(\mathbf{z}_{t+\Delta t}) = \hat{\mathbf{x}}_{t+\Delta t}, \end{aligned} \quad (10)$$

where $K^{\Delta t}$ is a finite dimensional, discrete-time representation of \mathcal{K}^t . This can be extended to control-affine systems by leveraging the KBF and encoding the invariant subspace of L_f and L_{g_i} s as

$$\begin{aligned} \mathbf{z}_t \approx \Psi_e(\mathbf{x}_t) &\rightarrow \mathbf{z}_{t+\Delta t} = e^{(A + \sum_{i=1}^m B_i u_{i_t}) \Delta t} \cdot \mathbf{z}_t \\ &\rightarrow \mathbf{x}_{t+\Delta t} \approx \Psi_d(\mathbf{z}_{t+\Delta t}) = \hat{\mathbf{x}}_{t+\Delta t}, \end{aligned} \quad (11)$$

assuming \mathbf{u}_t stays almost constant over Δt . Traditionally, since we are mostly interested in future prediction of the state, KAE is trained by minimizing the difference between $\hat{\mathbf{x}}_{t_0+(n+k)\Delta t}$ and $\mathbf{x}_{t_0+(n+k)\Delta t}$, with $n, k \in \mathbb{Z}_+ \cup \{0\}$. The loss functions traditionally used for training KAEs are the identity loss \mathcal{L}_{id} ($k = 0$), and the forward loss L_{fwd} ($k = 1, 2, \dots$) [18].

$$\mathcal{L}_{id} = \frac{1}{2M} \sum_{n=1}^M \|\hat{\mathbf{x}}_{t_0+n\Delta t} - \mathbf{x}_{t_0+n\Delta t}\|_2^2, \quad (12)$$

$$\mathcal{L}_{fwd} = \frac{1}{2k_m M} \sum_{k=1}^{k_m} \sum_{n=1}^M \|\hat{\mathbf{x}}_{t_0+(n+k)\Delta t} - \mathbf{x}_{t_0+(n+k)\Delta t}\|_2^2,$$

where $\|\cdot\|_2$ is the 2-norm, M is the number of samples over which we want to enforce the loss, and k_m is the maximum value of k , i.e. the maximum look-ahead step for multi-step training.

However, the KAE for control-affine system (11) has a *recurrent* structure which is exponential in control \mathbf{u}_t and linear in state \mathbf{z}_t . We use a first-order Euler discretization to maintain the bilinear recurrent structure in the KAE as

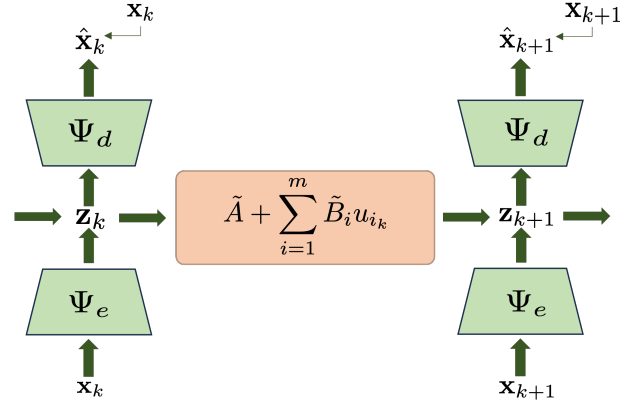


Fig. 1: Schematic of BLRAN (subscript k denotes the time-sample at $t_0 + k\Delta t$)

follows:

$$\begin{aligned} \mathbf{z}_{t+\Delta t} &= e^{(A + \sum_{i=1}^m B_i u_{i_t}) \Delta t} \cdot \mathbf{z}_t \\ &\approx (I_{N_l \times N_l} + A + \sum_{i=1}^m B_i u_{i_t}) \mathbf{z}_t \Delta t \\ &\approx \left(\tilde{A} + \sum_{i=1}^m \tilde{B}_i u_{i_t} \right) \mathbf{z}_t, \end{aligned} \quad (13)$$

where $\tilde{A} = (I_{N_l \times N_l} + A) \Delta t$ and $\tilde{B}_i = B_i \Delta t$. We call this autoencoder structure (Fig. 1) for control-affine system bilinearly recurrent autoencoder (BLRAN). While this architecture has not been formally defined in any previous literature, it has been applied for quadrotor trajectory tracking [11].

III. TEMPORALLY-CONSISTENT BILINEARLY RECURRENT AUTOENCODERS

This section describes our proposed temporally-consistent bilinearly recurrent autoencoder (tcBLRAN) architecture. The key idea is to introduce a consistency regularization term for training BLRAN as described for KAE in [12]. The fundamental idea derives from the time-invariance property of the control-affine systems. In the context of (7), the prediction consistency can be stated as the direct result of the following:

$$\begin{aligned} \mathbf{x}_{t_n} + \int_{t_n}^{t_n+k\Delta t} \left(\mathbf{f}(\mathbf{x}_t) + \sum_{i=1}^m \mathbf{g}_i(\mathbf{x}_t) u_{i_t} \right) dt \\ = \mathbf{x}_{t_n-k\Delta t} + \int_{t_n-k\Delta t}^{t_n+k\Delta t} \left(\mathbf{f}(\mathbf{x}_t) + \sum_{i=1}^m \mathbf{g}_i(\mathbf{x}_t) u_{i_t} \right) dt, \end{aligned} \quad (14)$$

$\forall n, k \in \mathbb{Z}_+ \cup \{0\}$, $k = 1, 2, \dots, n$, and $\mathbf{x}_{t_n} = \mathbf{x}_{t_0+n\Delta t}$. One key aspect of our approach is that instead of enforcing this consistency in the original state space, we do so in the Koopman invariant subspace (latent space). This helps avoid computation in the original high-dimensional space of nonlinear system, as well as provide robustness to noise. We justify enforcing such consistency in the latent space by summarizing the desired property of a consistent autoencoder Ψ_e and constructing the architecture of this framework. The

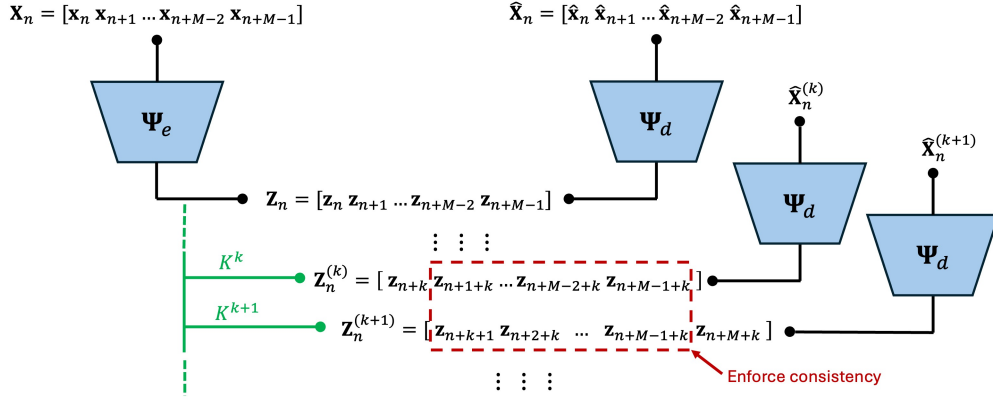


Fig. 2: Schematic of temporal consistency regularization (subscript k denotes the time-sample at $t_0 + k\Delta t$)

autoencoder $\Psi_e(\cdot) = [\psi_1(\cdot), \dots, \psi_{N_l}(\cdot)]$ defines a vector valued observable of the state space \mathbb{X} where each ψ_i is a scalar valued function. Let \mathcal{G} be the span of $\{\psi_1, \dots, \psi_{N_l}\}$. Lemma 1 summarizes the temporal consistency result under Assumption 1.

Assumption 1. The control input is assumed to be piecewise-constant, i.e., \mathbf{u}_t stays constant for a sampling interval Δt satisfying $\mathbf{u}_t = \mathbf{u}_n$ for $t \in [t_0 + n\Delta t, t_0 + (n+1)\Delta t)$.

Lemma 1. Let $\mathcal{G} = \text{span}\{\psi_1, \dots, \psi_{N_l}\}$ be invariant under L_f and L_{g_i} , $i = 1, \dots, m$. Let the state and control trajectories $\mathbf{x}_t, \mathbf{u}_t$ be sampled at time instances $\{t_0, t_0 + \Delta t, \dots, t_0 + n\Delta t, \dots\}$. Then for a piecewise-constant control \mathbf{u}_t as defined in Assumption 1, the following is true:

$$\begin{aligned} \mathbf{z}_t &= \Psi_e(\mathbf{x}_t) \\ \mathbf{z}_{t_0+(n+k)\Delta t} &= \prod_{\kappa=1}^k e^{(A + \sum_{i=1}^m B_i u_{i_{n+\kappa-1}})\Delta t} \mathbf{z}_{t_0+n\Delta t}, \end{aligned} \quad (15)$$

for all $n, k > 0$ and the product is carried out from right to left.

Proof. Since \mathcal{G} is invariant under L_f and L_{g_i} , $i = 1, \dots, m$, then the transformation $\mathbf{z}_t = \Psi_e(\mathbf{x}_t)$ satisfies the bilinear ODE:

$$\dot{\mathbf{z}}_t = A\mathbf{z}_t + \sum_{i=1}^m B_i \mathbf{z}_t u_{i_t}, \quad (16)$$

with some A, B_i , $i \in \{1, \dots, m\}$. Now, if the control input \mathbf{u}_t , $t \geq t_0$ is piecewise constant as described in Assumption 1, then, for the resultant latent-state trajectory \mathbf{z}_t satisfies

$$\mathbf{z}_{t_0+(n+1)\Delta t} = e^{(A + \sum_{i=1}^m B_i u_{i_n})\Delta t} \mathbf{z}_{t_0+n\Delta t},$$

for any time instance $t_0 + n\Delta t$. Now repeating this for k times we get the desired result. \square

Remark 2. The result in (15) can be approximated by first order Euler discretization as described in (13) to yield

$$\mathbf{z}_{t_0+(n+k)\Delta t} \approx \prod_{\kappa=1}^k \left(\tilde{A} + \sum_{i=1}^m \tilde{B}_i u_{i_{n+\kappa-1}} \right) \mathbf{z}_{t_0+n\Delta t}$$

Lemma 1 is essentially heart of the temporal consistency loss. In order to define our loss function, let us consider the reference time-step to be n . For a batch size of M (in latent space $\mathbf{Z}_n = [\mathbf{z}_{t_0+n\Delta t} \dots \mathbf{z}_{t_0+(n+M-1)\Delta t}]$), let the BLRAN advance the dynamics up to k_{tm} time-steps, giving rise to a set of batches $\mathbf{Z}_n^{(k)} = [\mathbf{z}_{t_0+(n+k)\Delta t}^{(k)}, \mathbf{z}_{t_0+(n+1+k)\Delta t}^{(k)}, \dots, \mathbf{z}_{t_0+(n+M+k-1)\Delta t}^{(k)}]$ with $k = 1, 2, \dots, k_{tm}$, where the superscript (k) denotes the multiplication with $\prod_{\kappa=1}^k \left(\tilde{A} + \sum_{i=1}^m \tilde{B}_i u_{i_{\kappa}} \right)$. The consistency loss \mathcal{L}_{ic} (Fig. 2) can be defined as,

$$\begin{aligned} \mathcal{L}_{ic} &= \frac{1}{2(k_{tm} - 1)} \sum_{q=1}^{k_{tm}-1} \mathcal{L}_q, \\ \mathcal{L}_q &= \frac{1}{(k_{tm} - q)} \sum_{k=1}^{k_{tm}-q} \mathcal{L}_k, \\ \mathcal{L}_k &= \frac{1}{(M - q)} \sum_{p=q}^{M-1} \|\mathbf{z}_{t_0+(n+k+p)\Delta t}^{(k)} - \mathbf{z}_{t_0+(n+k+p)\Delta t}^{(k+q)}\|^2 \end{aligned} \quad (17)$$

The total loss (\mathcal{L}_{tot}) for training tcBLRAN is given by,

$$\mathcal{L}_{tot} = \gamma_{id} \mathcal{L}_{id} + \gamma_{fwd} \mathcal{L}_{fwd} + \gamma_{tc} \mathcal{L}_{ic}, \quad (18)$$

Where γ_{id} , γ_{fwd} , and γ_{tc} are the corresponding scaling factors.

Remark 3. Temporal consistency loss \mathcal{L}_{ic} in (17) differs from the multi-step look-ahead prediction loss \mathcal{L}_{fwd} in (12) because the former compares among predictions from different initial conditions to same final time k_{tm} rather than comparing the predictions to different final time with the *labelled data*. Temporal consistency loss reduces BLRAN's dependence on large set of labelled training data.

Remark 4. While other KAE architectures [18] enforced consistency by exploiting the the time-reversible nature of autonomous dynamical systems, it fails for control systems due to its time-irreversible nature. Temporal consistency loss, however, does not require time-reversibility, thereby making it practical for maintaining consistency in KAE architecture for control systems.

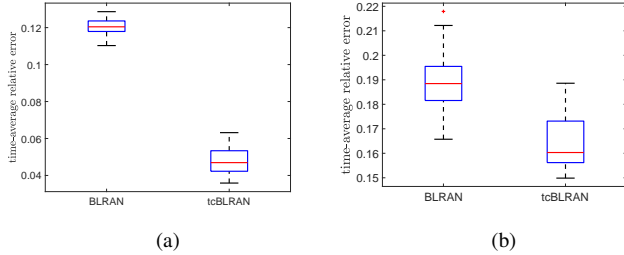


Fig. 3: Time-average relative prediction error for simple pendulum (20) over 30 initial conditions and 10 seeds: (a) Trained on clean data, (b) Trained on noisy data with 20 dB SNR.

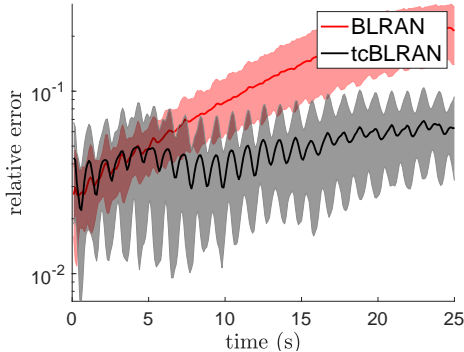


Fig. 4: Relative prediction error with time for simple pendulum (20)

IV. NUMERICAL EXAMPLES

The effectiveness tcBLRAN is demonstrated on three benchmark problems: the simple pendulum, Van der Pol oscillator, and forced Duffing oscillator. All three systems were simulated over the time interval $t = [0, 220]$ with a sampling interval of $\Delta t = 0.1s$, yielding 2200 equally spaced points. To mimic a high dimensional system, a random orthogonal transformation [18] is used to rotate each system to a higher dimensional space of 64 dimensions. Each system is simulated from initial condition $[0.8, 0]^\top$, and the time-average relative prediction error is calculated by simulating each system from 30 different initial conditions (taken as the last 30 points of the training dataset), with the control strategy employed being a piecewise-constant function with random scalar values in the range $[-0.15, 0.15]$. The relative prediction error is calculated over $T = 25s$ after rotating the state back to original dimension and is defined by

$$\text{error} = \frac{1}{T} \sum_{k=0}^{T-1} \frac{\|\hat{\mathbf{x}}_{t_0+k\Delta t} - \mathbf{x}_{t_0+k\Delta t}\|}{\|\mathbf{x}_{t_0+k\Delta t}\|}. \quad (19)$$

To assess the tcBLRAN's performance under different noise conditions, the networks for each system are trained with both clean data and noisy data with 20 dB SNR. In all three cases, tcBLRAN achieves superior prediction accuracy over the state of the art BLRAN for arbitrary piecewise constant control input. The tcBLRAN and BLRAN are trained and tuned over 10 different seeds for 600 epochs, and the learning rate decay is scheduled at epochs [30, 100, 200, 400]. Table I contains the training details.

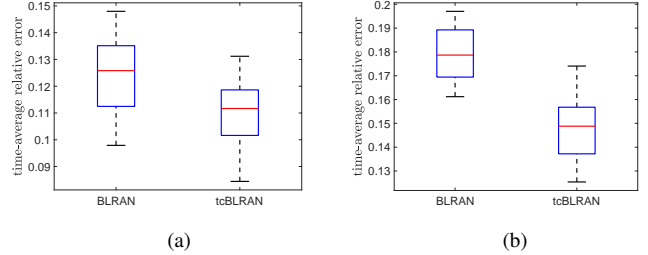


Fig. 5: Time-average relative prediction error for Van der Pol oscillator (21) over 30 initial conditions and 10 seeds: (a) Trained on clean data, (b) Trained on noisy data with 20 dB SNR.

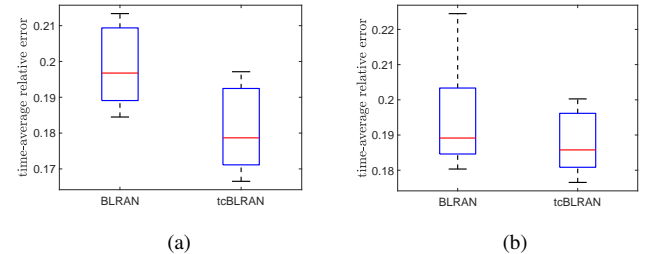


Fig. 6: Time-average relative prediction error for forced Duffing oscillator (22) over 30 initial conditions and 10 seeds: (a) Trained on clean data, (b) Trained on noisy data with 20 dB SNR.

A. Simple pendulum

The control-affine simple pendulum system, a canonical example in nonlinear dynamics, is modeled with the nonlinear equation

$$\ddot{\theta} + \frac{g}{l} \sin(\theta) = u, \quad (20)$$

where θ denotes the pendulum's angular displacement, $g = 9.8$ the gravitational acceleration, $l = 1$ the length of the pendulum, and u represents the control input. This is a two dimensional system with the state $[\theta \ \dot{\theta}]^\top$.

Time-averaged relative prediction error for 30 different initial conditions are depicted in Fig. 3 for clean and noisy data. Relative prediction error over 25s for clean training data of training length $N_{train} = 32$ is shown in Fig. 4.

B. Van der Pol oscillator

Next, tcBLRAN is applied to the controlled Van der Pol system [9]:

$$\dot{x} = \mu(1 - x^2)\dot{x} - x + u \quad (21)$$

The state $[x \ \dot{x}]^\top$ is again two-dimensional. The damping coefficient μ is set to 1. Time-average prediction errors are depicted in Fig. 5 for training length $N_{train} = 256$.

C. Forced Duffing oscillator

Lastly, tcBLRAN is used for modeling forced Duffing oscillator:

$$\ddot{x} = -\delta\dot{x} - \alpha x - \beta x^3 + u \quad (22)$$

with $\alpha = -1$, $\beta = 1$, and $\delta = 0.02$. Time-average prediction errors are shown in Fig. 6 with training length $N_{train} = 32$.

TABLE I: tcBLRAN (BLRAN) hyperparameters: hyphen(-) indicates same value

Hyperparameter	Value					
	Pendulum (20)		Van der Pol (21)		Duffing (22)	
	Clean	20 dB	Clean	20 dB	Clean	20 dB
SNR						
Learning rate	0.01 (-)	0.01 (-)	0.01 (-)	0.01 (-)	0.01 (-)	0.01 (-)
Learning rate decay	0.5 (-)	0.5 (-)	0.5 (-)	0.5 (-)	0.5 (-)	0.5 (-)
Weight decay	0.1 (0.01)	1 (-)	1 (-)	1 (-)	0.01 (0.1)	1 (-)
Gradient clipping	0.05 (-)	0.05 (-)	0.05 (-)	0.05 (-)	0.05 (-)	0.05 (-)
Look-ahead step k_m	12 (-)	12 (-)	32 (-)	32 (-)	12 (-)	12 (-)
Temporal consistency step k_{tm}	2 (N/A)	2 (N/A)	2 (N/A)	2 (N/A)	2 (N/A)	2 (N/A)
Batch size	32 (-)	32 (-)	64 (-)	64 (-)	32 (-)	32 (-)
γ_{id}	1 (-)	1 (-)	1 (-)	1 (-)	1 (-)	1 (-)
γ_{fwd}	1 (2)	0.5 (-)	1 (-)	2 (1)	2 (-)	2 (-)
γ_{tc}	2 (N/A)	0.5 (N/A)	0.01 (N/A)	2 (N/A)	0.5 (N/A)	0.5 (N/A)
Latent state dimension N_l	12 (-)	12 (-)	12 (-)	12 (-)	12 (-)	12 (-)
# Nodes $\Psi_e(\cdot)$	128 (-)	128 (-)	192 (-)	192 (-)	128 (-)	128 (-)
# Nodes $\Psi_d(\cdot)$	128 (-)	128 (-)	192 (-)	192 (-)	128 (-)	128 (-)

V. CONCLUSION

We present temporally-consistent bilinearly recurrent autoencoder (tcBLRAN) algorithm for accurately modeling a control-affine nonlinear system from state and input data. Despite its advantages, tcBLRAN has some limitations. Temporal consistency introduces computational overhead which increases training time. Furthermore, with sufficient training data, the performance gap between tcBLRAN and BLRAN narrows significantly. These trade-offs highlight the necessity of tcBLRAN in scenarios with scarce or noisy data, where its robustness and enhanced prediction accuracy provide a critical edge. This method combines the Koopman bilinear form (KBF) and the time-invariance property of the control-affine system to enforce temporal consistency in the latent variables with a bilinear latent dynamics. The tcBLRAN is evaluated and compared against the vanilla BLRAN on three systems with clean and noisy data. It outperforms the vanilla autoencoder methods for more accurate prediction which is important for control systems application. In future, the tcBLRAN model will be used for data-driven model-predictive control (MPC) of nonlinear system.

ACKNOWLEDGEMENT

The authors acknowledge the support of Ohio Supercomputer Center (PAS2709) for the computational resources.

REFERENCES

- [1] G. Hinton, L. Deng, D. Yu, G. E. Dahl, A. Mohamed, N. Jaitly, A. Senior, V. Vanhoucke, P. Nguyen, T. N. Sainath, and B. Kingsbury, "Deep neural networks for acoustic modeling in speech recognition: The shared views of four research groups," *IEEE Signal Processing Magazine*, vol. 29, no. 6, pp. 82–97, Nov 2012.
- [2] D. Silver, A. Huang, C. J. Maddison, A. Guez, L. Sifre, G. van den Driessche, J. Schrittwieser, I. Antonoglou, V. Panneershelvam, M. Lanctot, S. Dieleman, D. Grewe, J. Nham, N. Kalchbrenner, I. Sutskever, T. Lillicrap, M. Leach, K. Kavukcuoglu, T. Graepel, and D. Hassabis, "Mastering the game of Go with deep neural networks and tree search," *Nature*, vol. 529, no. 7587, pp. 484–489, 2016.
- [3] A. Fawzi, M. Balog, A. Huang, T. Hubert, B. Romera-Paredes, M. Barekatin, A. Novikov, F. J. R. Ruiz, J. Schrittwieser, G. Swirszcz, D. Silver, D. Hassabis, and P. Kohli, "Discovering faster matrix multiplication algorithms with reinforcement learning," *Nature*, vol. 610, no. 7930, pp. 47–53, 2022.
- [4] B. O. Koopman, "Hamiltonian systems and transformation in Hilbert space," *Proceedings of National Academy of Sciences*, vol. 17, pp. 315–318, 1931.
- [5] C. W. Rowley, I. Mezić, S. Bagheri, P. Schlatter, and D. S. Henningson, "Spectral analysis of nonlinear flows," *Journal of Fluid Mechanics*, vol. 641, pp. 115–127, 2009.
- [6] M. O. Williams, I. G. Kevrekidis, and C. W. Rowley, "A data-driven approximation of the Koopman operator: extending Dynamic Mode Decomposition," *Journal of Nonlinear Science*, vol. 25, no. 6, pp. 1307–1346, Dec 2015.
- [7] S. E. Otto and C. W. Rowley, "Linearly recurrent autoencoder networks for learning dynamics," *SIAM Journal on Applied Dynamical Systems*, vol. 18, no. 1, pp. 558–593, 2019.
- [8] B. Lusch, J. N. Kutz, and S. L. Brunton, "Deep learning for universal linear embeddings of nonlinear dynamics," *Nature communications*, vol. 9, no. 1, p. 4950, 2018.
- [9] D. Goswami and D. A. Paley, "Bilinearization, reachability, and optimal control of control-affine nonlinear systems: A koopman spectral approach," *IEEE Transactions on Automatic Control*, vol. 67, no. 6, pp. 2715–2728, 2022.
- [10] S. Peitz, S. E. Otto, and C. W. Rowley, "Data-driven model predictive control using interpolated Koopman generators," *SIAM Journal on Applied Dynamical Systems*, vol. 19, no. 3, pp. 2162–2193, 2020.
- [11] C. Folkestad, S. X. Wei, and J. W. Burdick, "Koopnet: Joint learning of koopman bilinear models and function dictionaries with application to quadrotor trajectory tracking," in *2022 International Conference on Robotics and Automation (ICRA)*, 2022, pp. 1344–1350.
- [12] I. Nayak, A. Chakrabarti, D. Goswami, M. Kumar, and F. Teixeira, "Temporally-consistent koopman autoencoders for forecasting dynamical systems," *arXiv preprint arXiv:2403.12335*, 2024.
- [13] A. Mauroy and I. Mezić, "Global stability analysis using the eigenfunctions of the Koopman operator," *IEEE Transactions on Automatic Control*, vol. 61, no. 11, pp. 3356–3369, Nov 2016.
- [14] R. Mohr and I. Mezić, "Construction of eigenfunctions for scalar-type operators via Laplace averages with connections to the Koopman operator," *ArXiv e-prints*, Mar. 2014.
- [15] M. Budisić, R. Mohr, and I. Mezić, "Applied Koopmanism," *Chaos: An Interdisciplinary Journal of Nonlinear Science*, vol. 22, no. 4, 2012.
- [16] D. Goswami and D. A. Paley, "Global bilinearization and controllability of control-affine nonlinear systems: A Koopman spectral approach," in *2017 IEEE 56th Annual Conference on Decision and Control*, Dec 2017, pp. 6107–6112.
- [17] N. Takeishi, Y. Kawahara, and T. Yairi, "Learning koopman invariant subspaces for dynamic mode decomposition," *Advances in neural information processing systems*, vol. 30, 2017.
- [18] O. Azencot, N. B. Erichson, V. Lin, and M. Mahoney, "Forecasting sequential data using consistent koopman autoencoders," in *International Conference on Machine Learning*. PMLR, 2020, pp. 475–485.